Neutrino luminosity and matter-induced modification of collective neutrino flavor oscillations in supernovae

John F. Cherry, Meng-Ru Wu, J. Carlson, Huaiyu Duan, George M. Fuller, and Yong-Zhong Qian

Phys. Rev. D **85**, 125010 — Published 7 June 2012

DOI: 10.1103/PhysRevD.85.125010

Neutrino Luminosity and Matter-Induced Modification of Collective Neutrino Flavor Oscillations in Supernovae

John F. Cherry,[1,2] Meng-Ru Wu,[3] J. Carlson,[4,2] Huaiyu Duan,[5,2] George M. Fuller,[1,2] and Yong-Zhong Qian[3]

[1]*Department of Physics, University of California, San Diego, La Jolla, California 92093, USA*

[2]*Neutrino Engineering Institute, New Mexico Consortium, Los Alamos, New Mexico 87545, USA*

[3]*School of Physics and Astronomy, University of Minnesota, Minneapolis, MN 55455, USA*

[4]*Theoretical Division, Los Alamos National Laboratory, Los Alamos, New Mexico 87545, USA*

[5]*Department of Physics and Astronomy, University of New Mexico, Albuquerque, New Mexico 87131, USA*

Abstract

We present the first calculations of self-coupled neutrino flavor oscillations with time integrated luminosities and energy spectra for the neutronization burst of an O-Ne-Mg core-collapse supernova. These calculations allow us to gauge the effects of time varying neutrino luminosity and of the bump in the electron number density profile at the base of the hydrogen envelope in O-Ne-Mg core-collapse supernovae. The bump allows a significant fraction of the low-energy ν_e to survive by rendering their flavor evolution nonadiabatic. Increasing the luminosity of the neutronization burst shifts the bump-affected ν_e to lower energy with reduced survival probability. Similarly, lowering the luminosity shifts the bump-affected neutrinos to higher energies. While these low energy neutrinos lie near the edge of detectability, the population of bump-affected neutrinos has direct influence on the spectral swap formation in the neutrino signal at higher energies.

PACS numbers: 14.60.Pq, 97.60.Bw

I. INTRODUCTION

Stars of ~ 8–$10\,M_\odot$ ($M_\odot$ being the mass of the sun) develop O-Ne-Mg cores at the end of their evolution. Capture of electrons by the Ne and Mg isotopes initiates the gravitational collapse of the core, which eventually produces a supernova and leaves behind a neutron star [1, 2]. These O-Ne-Mg core-collapse supernovae are the only case for which the neutrino-driven mechanism has been demonstrated to work by different groups [3, 4]. The success of this mechanism is largely due to the steep fall-off of the matter density above the core. As shown by Refs. [5–8], this special density structure also provides a venue where neutrino flavor transformation occurs under the influence of both neutrino-electron and neutrino-neutrino forward scatterings [9–27]. In particular, the neutronization burst, which consists predominantly of ν_e and signifies the breakthrough of the neutrino sphere by the supernova shock, experiences interesting flavor evolution including collective oscillations for the neutrino flavor mixing parameters found by experiments [28].

In this paper we explore another special feature of the matter structure in O-Ne-Mg core-collapse supernovae in connection with flavor evolution of the neutronization neutrino burst. The hydrogen envelope has an electron fraction of $Y_e \approx 0.85$. In contrast, the material below the envelope has $Y_e \approx 0.5$, reflecting weak interaction-induced neutronization during pre-supernova evolution. As the matter density ρ is a continuous function of radius, this produces a bump in the electron number density $n_e = \rho Y_e N_A$ (N_A being Avogadro's number) at the base of the hydrogen envelope, shown explicitly in Ref. [8]. As noted in Refs. [5–8], for the normal neutrino mass hierarchy, this bump renders flavor evolution of the low-energy ν_e in the neutronization burst nonadiabatic, giving rise to substantial survival probabilities for these ν_e. Here we show that this bump facilitates an interesting interplay between neutrino-electron and neutrino-neutrino forward scattering in the flavor evolution of the low-energy ν_e, and we show how this influences the collective oscillations of neutrinos at higher energies.

II. NEUTRONIZATION BURST NEUTRINOS

We assume a pure ν_e burst emitted from the neutrino sphere at $R_\nu = 60$ km with a total luminosity $L_\nu = 10^{52} - 10^{54}\,\mathrm{erg\,s^{-1}}$ and a normalized spectrum

$$f_\nu(E) = \frac{1}{F_2(\eta_\nu) T_\nu^3} \frac{E^2}{\exp(E/T_\nu - \eta_\nu) + 1}, \tag{1}$$

where we take $\eta_\nu = 3$ and $T_\nu = 2.75$ MeV [corresponding to an average ν_e energy $\langle E_\nu \rangle = F_3(\eta_\nu)T_\nu/F_2(\eta_\nu) = 11$ MeV at emission]. Here

$$F_n(\eta) = \int_0^\infty \frac{x^n}{\exp(x-\eta)+1} dx. \tag{2}$$

In the single-angle approximation, the neutrino-neutrino forward scattering potential can be written in terms of an *effective* total neutrino number density at $r > R_\nu$,

$$n_\nu(r) = \frac{L_\nu}{4\pi R_\nu^2 \langle E_\nu \rangle} \left[1 - \sqrt{1-(R_\nu/r)^2}\right]^2 \approx \frac{L_\nu R_\nu^2}{16\pi \langle E_\nu \rangle r^4}, \tag{3}$$

where the approximate equality holds for $r \gg R_\nu$.

For the purposes of this study we have chosen the following neutrino mixing parameters: neutrino mass squared differences $\Delta m^2_\odot = 7.6 \times 10^{-5}\,\mathrm{eV}^2$ and $\Delta m^2_{\rm atm} = 2.4 \times 10^{-3}\,\mathrm{eV}^2$; vacuum mixing angles $\theta_{12} = 0.59$, $\theta_{23} = \pi/4$, $\theta_{13} = 0.1$; and CP-violating phase $\delta = 0$. We employ multi-angle neutrino flavor transformation calculations, which specifically treat neutrinos emitted at different angles relative to the surface of the neutrinosphere and separately follow their flavor evolution.

Initially, we will concentrate on the normal neutrino mass hierarchy, because previous work has shown that mixing at the $\Delta m^2_{\rm atm}$ scale with this heirarchy produces interesting collective neutrino flavor oscillations in O-Ne-Mg core-collapse supernovae [5–8]. For the atmospheric neutrino mass doublet with an inverted hierarchy, neutrinos in the neutronization burst do not experience any flavor transformation.

The results from multi-angle simulations in Figures 1 and 2, which show the final neutrino spectra as a flux weighted average over all emission angle trajectories, demonstrate that the n_e profile with the bump gives rise to a very clear flavor transformation signature. Note that the flavor swaps shown in Figures 1 and 2 are spread out in energy space. This is a feature of multi-angle calculations, where slight differences in swap energy across different emission angle trajectories spreads out the swap transition, and the sharp swap features of single-angle calculations are gone. This makes swaps slightly more difficult to resolve in a detected neutronization neutrino burst signal. Depending on the luminosity, a population of ν_e below 8 MeV have large probabilities to transform between neutrino mass states (have large hopping probabilities). For example, the medium range luminosity case, $L_\nu = 8.0 \times 10^{52}\,\mathrm{erg\,s^{-1}}$, exhibits a peak hopping probability for the bump-affected neutrinos of $\sim 55\%$ at $E_\nu = 3.1\,\mathrm{MeV}$, shown in Figure 2. In the extreme case of $L_\nu = 10^{54}\,\mathrm{erg\,s^{-1}}$, the hopping

probability is $\sim 15\%$ for $E_\nu = 0.5\,\mathrm{MeV}$, although this is hard to see in Figure 1 (but see Figure 2).

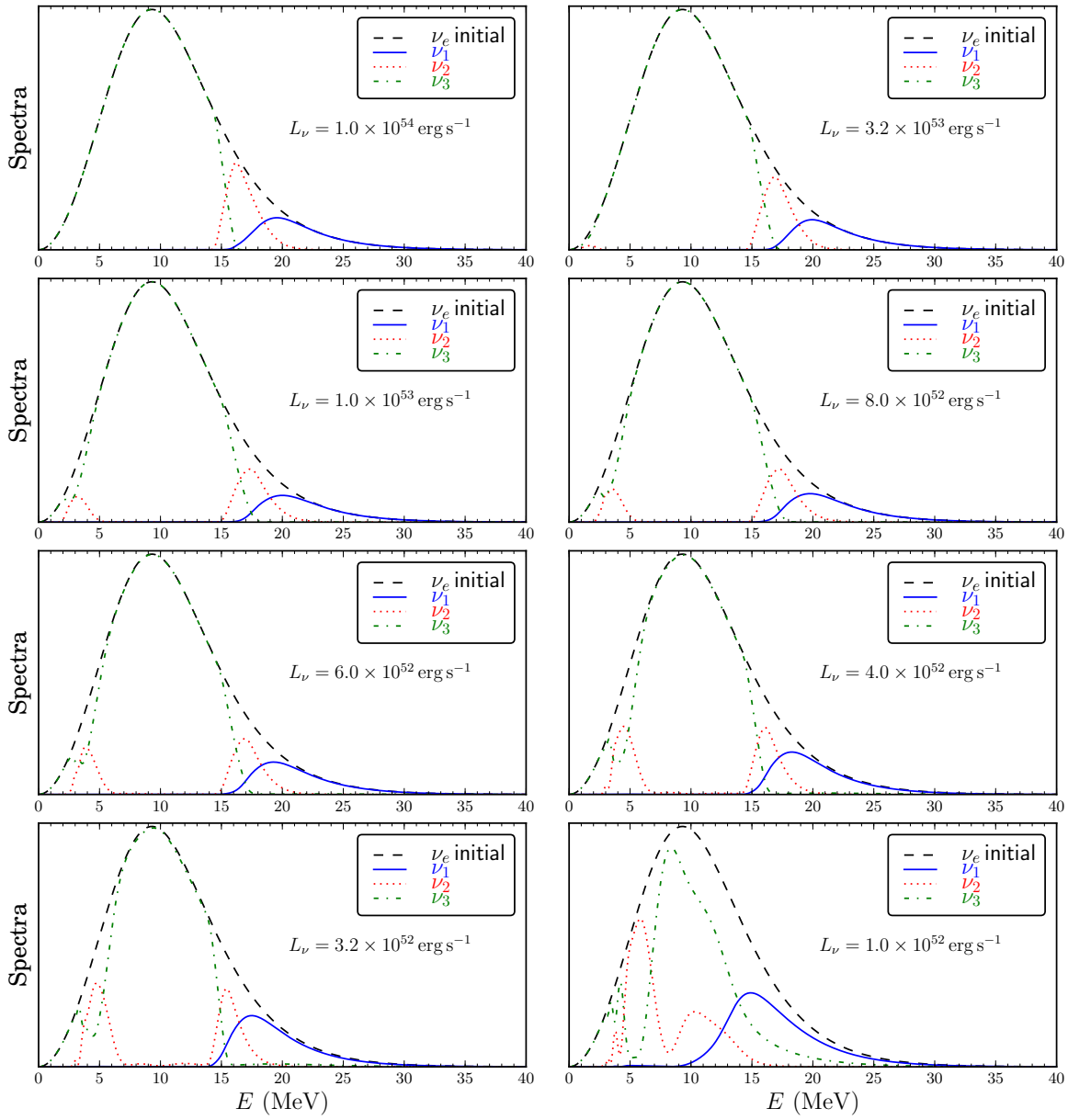

FIG. 1: The final emission angle averaged neutrino mass state energy spectra for calculations of the flavor transformation in the neutronization neutrino burst of an O-Ne-Mg core-collapse supernova. Each panel shows the results for a different possible burst luminosity, ranging from $L_\nu = 10^{54} - 10^{52}\,\mathrm{erg\,s^{-1}}$, with identical Fermi-Dirac energy distributions.

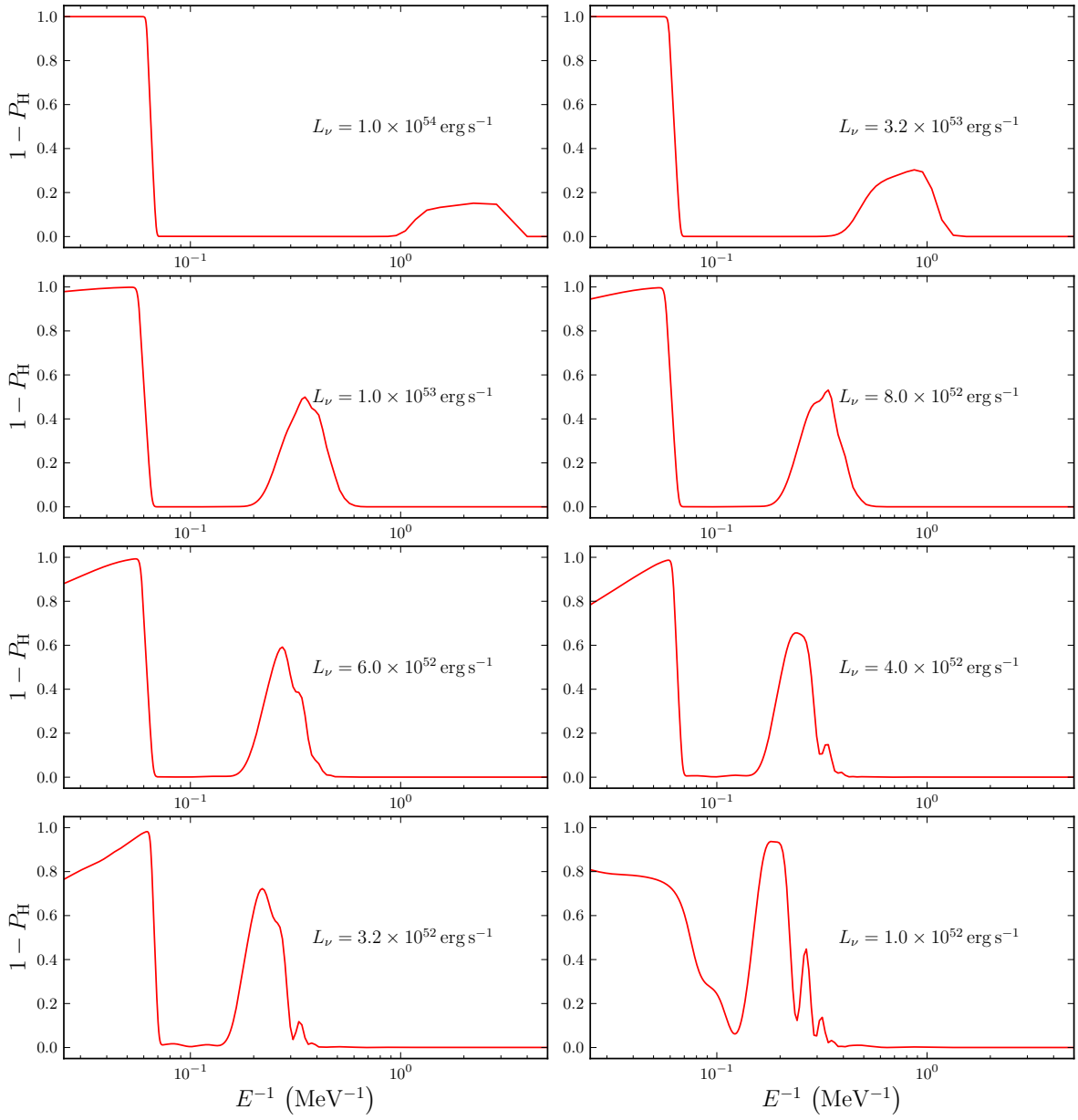

FIG. 2: The emission angle averaged probability for electron neutrinos in the neutronization neutrino burst of an O-Ne-Mg core-collapse supernova to hop out of the (initial) heavy mass eigenstate, $1-P_{\rm H}$, plotted as a function of inverse neutrino energy. Each panel shows the results for a different possible burst luminosity, ranging from $L_\nu = 10^{54} - 10^{52}\,{\rm erg\,s^{-1}}$, with identical Fermi-Dirac energy distributions.

III. ANALYSIS OF FLAVOR EVOLUTION OF THE ν_e's

As discussed in Refs. [5–8] the flavor evolution of the ν_e flux in this case is governed by $\delta m^2_{\rm atm}$ and θ_{13}. Although the numerical calculations we have conducted employ full 3×3 flavor mixing, in the following analysis, we focus on the 2-flavor mixing for these ν_e with $\delta m^2 = \delta m^2_{\rm atm}$ and $\theta_{\rm v} = \theta_{13}$. Further, we adopt the single-angle approximation, as this has been shown to be effective in providing qualitative understanding of the results from multi-angle simulations.

Using the notation introduced in Ref. [29], we can represent a ν_e of energy E by a neutrino flavor isospin (NFIS) $\mathbf{s}_\omega$ with $\omega = \delta m^2/2E$. The evolution of $\mathbf{s}_\omega$ is governed by

$$\frac{d}{dr}\mathbf{s}_\omega = \mathbf{s}_\omega \times \left[\omega \mathbf{H}_{\rm v} + \mathbf{H}_e - \mu(r) \int_0^\infty \mathbf{s}_{\omega'} f_\nu(E_{\omega'}) dE_{\omega'}\right], \tag{4}$$

where $\mathbf{H}_{\rm v} = \cos 2\theta_{\rm v} \hat{\mathbf{e}}^{\rm f}_z - \sin 2\theta_{\rm v} \hat{\mathbf{e}}^{\rm f}_x$, $\mathbf{H}_e = -\sqrt{2} G_F n_e(r) \hat{\mathbf{e}}^{\rm f}_z$, $\mu(r) = 2\sqrt{2} G_F n_\nu(r)$, and $E_{\omega'} = \delta m^2/2\omega'$. Here $\hat{\mathbf{e}}^{\rm f}_x$ and $\hat{\mathbf{e}}^{\rm f}_z$ are the unit vectors in the x and z directions, respectively, of the neutrino flavor space. For convenience, we define

$$g(\omega) \equiv \frac{\delta m^2}{2\omega^2} f_\nu(E_\omega) \tag{5}$$

and

$$\mathbf{S} \equiv \int_0^\infty \mathbf{s}_\omega f_\nu(E_\omega) dE_\omega = \int_0^\infty \mathbf{s}_\omega g(\omega) d\omega. \tag{6}$$

It follows that

$$\frac{d}{dr}\mathbf{S} = \int_0^\infty \omega g(\omega) \mathbf{s}_\omega d\omega \times \mathbf{H}_{\rm v} + \mathbf{S} \times \mathbf{H}_e. \tag{7}$$

As $g(\omega)$ is concentrated in a finite range of ω, to zeroth order we approximate $g(\omega) \approx \delta(\omega - \langle\omega\rangle)$, where $\langle\omega\rangle = \int_0^\infty \omega g(\omega) d\omega$ is calculated from the actual $g(\omega)$ in Eq. (5). Then the zeroth-order mean field $\mathbf{S}^{(0)}$ can be obtained from

$$\frac{d}{dr}\mathbf{S}^{(0)} = \mathbf{S}^{(0)} \times [\langle\omega\rangle \mathbf{H}_{\rm v} + \mathbf{H}_e] \equiv \mathbf{S}^{(0)} \times \mathbf{H}_{\rm MSW}. \tag{8}$$

The evolution of $\mathbf{S}^{(0)}$ is the same as that of a ν_e with $E_{\rm MSW} = \delta m^2/2\langle\omega\rangle = 8.53$ MeV undergoing the usual MSW effect. With this, we can approximately solve the evolution of $\mathbf{s}_\omega$ by employing

$$\frac{d}{dr}\mathbf{s}_\omega \approx \mathbf{s}_\omega \times \left[\omega \mathbf{H}_{\rm v} + \mathbf{H}_e - \mu(r) \mathbf{S}^{(0)}\right]. \tag{9}$$

As the heavy mass eigenstate essentially coincides with ν_e at high densities, but the light mass eigenstate is predominantly ν_e at low densities, the survival probability of an initial

ν_e is approximately $1 - P_{\rm H}$, where $P_{\rm H}$ is the probability for remaining in the heavy mass eigenstate.

A. Dependence on L_ν

We can go further by using the zeroth-order mean field $\mathbf{S}^{(0)}$ to understand how the flavor evolution of the low-energy ν_e depends on L_ν. As discussed below, Equations 8 and 9 imply that neutrinos with $\omega \gg \langle\omega\rangle$ will experience an MSW resonance before the resonance of $\mathbf{S}^{(0)}$. These higher frequency neutrinos may pass through multiple resonances created by the matter potential bump.

Based on the MSW effect, $\mathbf{S}^{(0)}$ corresponding to $E_{\rm MSW} = 8.53$ MeV goes through the resonance after the low-energy ν_e. Assuming adiabatic evolution of $\mathbf{S}^{(0)}$ before the resonance, we can take

$$\mathbf{S}^{(0)} \approx -\frac{\mathbf{H}_{\rm MSW}}{2|\mathbf{H}_{\rm MSW}|} \approx -\frac{1}{2}(\cos 2\theta_m \hat{\mathbf{e}}_z^f - \sin 2\theta_m \hat{\mathbf{e}}_x^f), \tag{10}$$

where

$$\cos 2\theta_m = \frac{\langle\omega\rangle \cos 2\theta_{\rm v} - \sqrt{2}G_F n_e}{\sqrt{(\langle\omega\rangle \cos 2\theta_{\rm v} - \sqrt{2}G_F n_e)^2 + (\langle\omega\rangle \sin 2\theta_{\rm v})^2}}, \tag{11}$$

$$\sin 2\theta_m = \frac{\langle\omega\rangle \sin 2\theta_{\rm v}}{\sqrt{(\langle\omega\rangle \cos 2\theta_{\rm v} - \sqrt{2}G_F n_e)^2 + (\langle\omega\rangle \sin 2\theta_{\rm v})^2}}. \tag{12}$$

The evolution of $\mathbf{s}_\omega$ before the resonance of $\mathbf{S}^{(0)}$ is then governed by

$$\frac{d}{dr}\mathbf{s}_\omega \approx \mathbf{s}_\omega \times \left[(\omega \cos 2\theta_{\rm v} - \sqrt{2}G_F n_e + \frac{\mu}{2}\cos 2\theta_m)\hat{\mathbf{e}}_z^f - (\omega \sin 2\theta_{\rm v} + \frac{\mu}{2}\sin 2\theta_m)\hat{\mathbf{e}}_x^f\right] \tag{13}$$

$$\equiv \mathbf{s}_\omega \times \mathbf{H}_\omega. \tag{14}$$

The above equation shows that $\mathbf{s}_\omega$ goes through the resonance when

$$\omega \cos 2\theta_{\rm v} = \sqrt{2}G_F n_e - \frac{\mu}{2}\cos 2\theta_m \equiv |{\rm H}_e| + B. \tag{15}$$

Note that $\cos 2\theta_m < 0$ before the resonance of $\mathbf{S}^{(0)}$ [see Eq. (11)] and therefore $B > 0$. Consequently, the energy of those ν_e ($E_\omega = \delta m^2/2\omega$) that go through the resonance at the bump in the n_e profile decreases as L_ν, and hence B, increases. This trend can be seen in every frame in Figures 1 and 2. As the neutrino luminosity is increased, the peak energy of the population of low energy neutrinos that hop out of the heavy neutrino mass eigenstate as a result of the bump decreases.

We can also qualitatively understand why increasing L_ν produces a decreasing survival probability of the bump-affected ν_e. The Landau-Zener probability for hopping from the heavy to the light mass eigenstate after the resonance is

$$P_{\rm hop} = \exp\left[-\frac{\pi}{4}\frac{\delta m^2 \sin^2 2\theta_{\rm v}}{E\cos 2\theta_{\rm v}}\mathcal{H}_{\rm res}\right], \tag{16}$$

where

$$\mathcal{H}_{\rm res} \equiv \left|\frac{d\ln(|{\rm H}_e| + B)}{dr}\right|^{-1}_{\rm res} \tag{17}$$

is the scale height of the total flavor-evolution potential at the resonance position. Crudely we have $1 - P_{\rm H} \sim P_{\rm hop}$. As increasing L_ν shifts the resonance energy window to lower E_ν at the bump in the n_e profile, $P_{\rm hop}$ decreases because flavor evolution through the resonance tends to be more adiabatic for lower-energy neutrinos [see Eq. (16)]. In addition, as B decreases much more slowly than $|{\rm H}_e|$ with radius, $\mathcal{H}_{\rm res}$ becomes larger when the contribution from B increases with L_ν. This also reduces $P_{\rm hop}$ [see Eq. (16)].

Furthermore, equations (8) and (9) also imply that a sufficiently large neutrino-neutrino scattering potential will cause neutrinos with oscillation frequencies roughly equal to or less than $\langle\omega\rangle$ to follow the evolution of $\mathbf{S}^{(0)}$ as this vector moves through resonance. To illustrate this, we choose to define the angle α as the angle between $\mathbf{H}_{\rm MSW}$ and either $\mathbf{S}^{(0)}$ or $\mathbf{S}$. The heavy mass eigenstate survival probability $P_{\rm H}$ of the collective ensemble of neutrinos that follow the evolution of $\mathbf{S}^{(0)}$ is related to α by

$$P_{\rm H} = 1 - \frac{1}{2}\left(1 + \cos\alpha\right). \tag{18}$$

Figure 3 shows the evolution of α for the simulations with relatively high luminosities. From the figure it can be seen that the evolution of $\mathbf{S}$ for these luminosities is qualitatively similar to that of $\mathbf{S}^{(0)}$.

Interestingly, the final alignment angle, α, for the collective neutrino isospin vectors is slightly larger than it is for $\mathbf{S}^{(0)}$. This means that the collective NFIS's are more closely aligned with $-\hat{\mathbf{H}}_{\rm v}$ than $\mathbf{S}^{(0)}$ is. The highest luminosity simulation, with $L_\nu = 10^{54}\,{\rm erg\,s^{-1}}$, has the collective NFIS that is most closely aligned with $\mathbf{S}^{(0)}$, and the reason for this can be found in Eq. 9. In the limit of $\mu\,(r) \gg |\mathbf{H}_{\rm e}| \gg \omega$ the individual $\mathbf{s}_\omega$ will orbit exclusively around $\mathbf{S}^{(0)}$ and follow it through resonance. However, it can be seen from Eqs. 11 and 13 that only neutrinos with $\omega = \langle\omega\rangle$ go through resonance at the exact position where $\cos 2\theta_{\rm m} = 0$. Neutrinos following the evolution of $\mathbf{S}^{(0)}$ will still experience some fraction of the neutrino

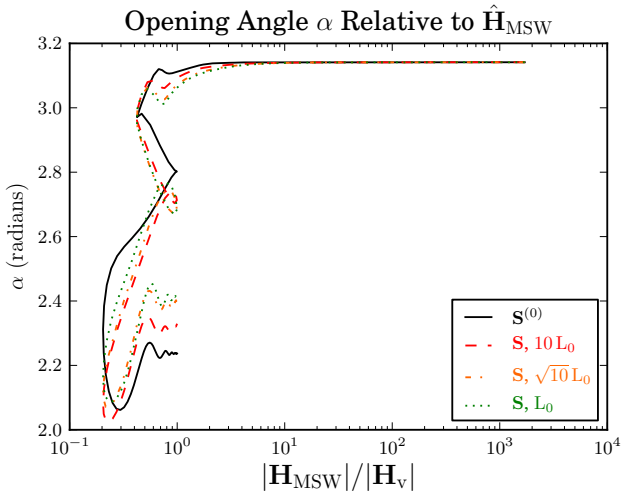

FIG. 3: High luminosity evolution ($L_0 = 10^{53}\,\mathrm{erg\,s^{-1}}$): The opening angle α between the collective NFIS $\mathbf{S}^{(0)}$ and $\mathbf{H}_{\rm MSW}$, plotted as a function of $|\mathbf{H}_{\rm MSW}|\,/\,|\mathbf{H}_{\rm v}|$ as the system moves through resonance. The idealized NFIS (solid line) shows the evolution of $\mathbf{S}^{(0)}$ in the ideal, strong neutrino self-coupling case. The dashed line, dot-dashed line, and dotted line show the evolution of $\mathbf{S}$ as calculated for neutrino luminosities $10L_0$, $\sqrt{10}L_0$, and L_0 respectively.

self-coupling potential, although at resonance $|\mathbf{H}_{\rm e}| \gg B$ for neutrinos that track $\mathbf{S}^{(0)}$. This results in a small increase in $\mathcal{H}_{\rm res}$, which slightly lowers the overall hopping probability and slightly increases α.

When the neutrino luminosity is moderately lower, the same basic phenomenon is observed. Figure 4 shows the evolution of α for the simulations with moderate luminosities, $0.6 - 1.0 \times 10^{53}\,\mathrm{erg\,s^{-1}}$. The collective NFIS $\mathbf{S}$ for these simulations still tracks roughly the evolution of $\mathbf{S}^{(0)}$, although deviations become more pronounced as the neutrino luminosity decreases. Counter-intuitively, the final alignment of the lower luminosity $\mathbf{S}$'s is closer to that of $\mathbf{S}^{(0)}$ than in the calculations with $L_\nu = 10^{53}\,\mathrm{erg\,s^{-1}}$. This effect originates in the contribution of the bump-affected neutrinos to the integrals in Eqs. 6 and 7. From Figure 1 one can see that the population of bump-affected neutrinos has grown appreciably in this luminosity range, comprising $7 - 10\,\%$ of all neutrinos. These bump affected neutrinos are not connected in a coherent fashion to the flavor evolution of $\mathbf{S}$, but they are predominantly aligned with the $+\hat{\mathbf{H}}_{\rm v}$ axis (they are predominantly ν_2). This means that they will tend to drag the alignment of $\mathbf{S}$ closer to the $+\hat{\mathbf{H}}_{\rm v}$ axis, which systematically moves the final value of α lower.

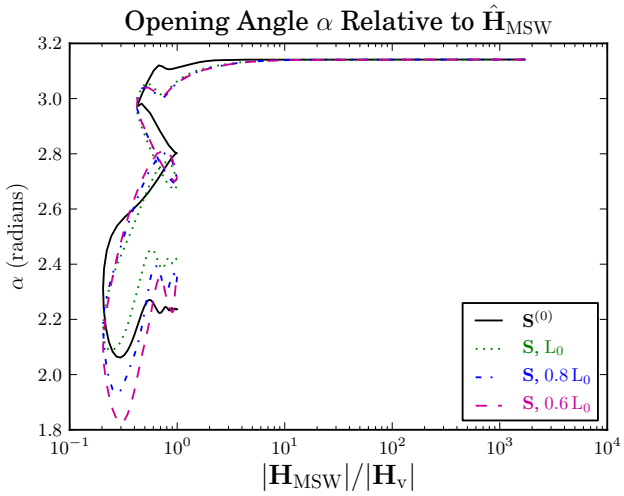

FIG. 4: Moderate luminosity evolution ($L_0 = 10^{53}\,\mathrm{erg\,s^{-1}}$): The opening angle α between the collective NFIS $\mathbf{S}^{(0)}$ and $\mathbf{H}_{\rm MSW}$, plotted as a function of $|\mathbf{H}_{\rm MSW}|\,/\,|\mathbf{H}_{\rm v}|$ as the system moves through resonance. The idealized NFIS (solid line) shows the evolution of $\mathbf{S}^{(0)}$ in the ideal, strong neutrino self-coupling case. The dashed line, dot-dashed line, and dotted line show the evolution of $\mathbf{S}$ as calculated for neutrino luminosities L_0, $0.8\,L_0$, and $0.6\,\mathrm{L}_0$ respectively.

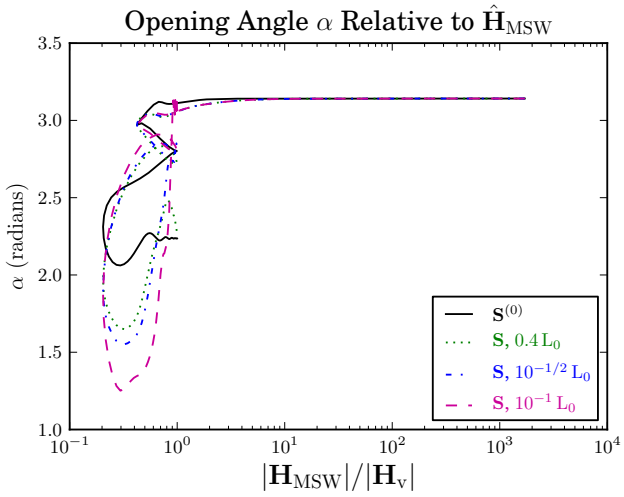

FIG. 5: Low luminosity evolution ($L_0 = 10^{53}\,\mathrm{erg\,s^{-1}}$): The opening angle α between the collective NFIS $\mathbf{S}^{(0)}$ and $\mathbf{H}_{\rm MSW}$, plotted as a function of $|\mathbf{H}_{\rm MSW}|\,/\,|\mathbf{H}_{\rm v}|$ as the system moves through resonance. The idealized NFIS (solid line) shows the evolution of $\mathbf{S}^{(0)}$ in the ideal, strong neutrino self-coupling case. The dashed line, dot-dashed line, and dotted line show the evolution of $\mathbf{S}$ as calculated for neutrino luminosities $0.4\,L_0$, $10^{-1/2}\,L_0$, and $10^{-1}\,\mathrm{L}_0$ respectively.

For luminosities below $L_\nu = 6.0 \times 10^{52}\,\mathrm{erg\,s^{-1}}$, the magnitude of the neutrino self-coupling potential drops below $\langle\omega\rangle = 1.4 \times 10^{-16}\,\mathrm{MeV}$ prior to reaching the resonance region of $\mathbf{S}^{(0)}$. This means that many neutrino states will undergo an MSW-like flavor transformation prior to reaching this region of the supernova envelope. As a result, these neutrinos, including those with $\omega = \langle\omega\rangle$, will not participate in the collective flavor oscillations we have described. In turn, this means that the approximation $g(\omega) \approx \delta(\omega - \langle\omega\rangle)$ is not justified in this case. Ultimately this approximation breaks down because the evolution of the neutrino state with $\omega = \langle\omega\rangle$ is not coherently related to the evolution of other neutrino flavor states.

The progressive breakdown of this approximation with decreasing neutrino luminosity can be seen in Figure 5. The motion of the vector $\mathbf{S}$ for each calculation deviates widely from the motion of $\mathbf{S}^{(0)}$. Furthermore, the final alignment angle α for each $\mathbf{S}$ is no longer related to the actual hopping probability for neutrinos in those calculations. The hopping probability inferred from Figure 5 and Equation (18) differs dramatically from the actual hopping probability observed in the calculations shown in Figures 1 and 2 for low L_ν. The discrepancies are $\Delta P_{\mathrm{hop}} = 0.16,\ 0.35,\ 0.48$ for the calculations with $L_\nu = 4.0,\ \sqrt{10},\ 1.0 \times 10^{52}\,\mathrm{erg\,s^{-1}}$ respectively.

B. Spectral Swap Formation

If the luminosity is large enough, it can be seen that after the neutrinos in these calculations have passed the resonance region, the neutrino self-coupling potential becomes the dominant term in the neutrino forward scattering potential. Neutrinos which have $\omega < \mu(r)$ fall into a form of collective flavor oscillations known as the Regular Precession mode. The Regular Precession mode is typified by the collective ensemble of neutrinos rotating with a common frequency, ω_{pr} about the axis of the vacuum mass basis,

$$\frac{d}{dr}\mathbf{s}_\omega = \omega_{\mathrm{pr}}\left(\mathbf{s}_\omega \times \mathbf{H}_{\mathrm{v}}\right). \tag{19}$$

This collective oscillation has the feature that it conserves an effective lepton number (or "energy") of the ensemble of neutrinos. While this lepton number has a more complicated general expression, in the particular case of the neutronization neutrino burst where the initial flux of neutrinos is nearly pure ν_{e}, the conserved lepton number is simply $\propto n_\nu P_{\mathrm{H}}$ for neutrino mixing at the atmospheric mass scale.

In the initial stages of neutrino flavor transformation, this lepton number is not conserved. However, thereafter the Regular Precession mode fixes the total number of neutrinos in mass state 3. This gives the criterion for the precession frequency, $\omega_{\rm pr}$, for the system,

$$\int_{\omega_{\rm pr}}^{\infty} P_H\left(\omega\right) g\left(\omega\right) d\omega = \int_{0}^{\infty} g\left(\omega\right) \{P_H\left(\omega\right) - \left[P_2\left(\omega\right) + P_1\left(\omega\right)\right]\} d\omega, \tag{20}$$

where $P_1\left(\omega\right),\ P_2\left(\omega\right)$ are the probabilities of a neutrino with oscillation frequency ω to be in the instantaneous mass eigenstate 1, or 2 respectively.

It is this precession frequency that sets the energy of the spectral swap (in this case between mass state 3 and mass state 2). As the magnitude of the self coupling drops, neutrinos with oscillation frequencies in the range $\mu\left(r\right) > \omega > \omega_{\rm pr}$ will participate in the Regular Precession mode and will align with mass state 3, while neutrinos with $\omega < \omega_{\rm pr}$ will be aligned with mass state 2. The final results of this process can be seen in Figure 1. For all but the least luminous calculation a spectral swap forms, with $E_{\rm swap} = \delta m^2/2\omega_{\rm pr}$, close to $E_\nu \sim 15\,{\rm MeV}$. The precise location of $E_{\rm swap}$ depends on the details of flavor transformation due to the motion of $\mathbf{S}^{(0)}$ and the bump affected neutrinos. Broadly speaking, a smaller $P_{\rm H}$ found from Eq. 18 will lower the swap energy of the final neutrino energy spectra by reducing the value of the integral on the right side of Eq. 20. However, a larger population of bump affected neutrinos will move the swap energy to higher values (smaller $\omega_{\rm pr}$) by reducing $P_{\rm H}\left(\omega\right) g\left(\omega\right)$ for large ω.

It is important to note that the spectral swap between mass states 3 and 2 can sometimes form even when the coherent flavor evolution of neutrinos has broken down deeper in the envelope. As discussed in the previous section, for the calculations with $L_\nu < 6.0 \times 10^{52}\,{\rm erg\,s^{-1}}$ collective neutrino flavor transformation breaks down in the resonance region because $\mu\left(r\right) < \langle\omega\rangle$. However, from Figure 1 it can be seen that a mass state 3/2 swap still forms successfully for $L_\nu = 4.0 \times 10^{52}\,{\rm erg\,s^{-1}}$ and $L_\nu = \sqrt{10} \times 10^{52}\,{\rm erg\,s^{-1}}$. Swaps between mass state 3 and 2 form for these two models where the luminosity is low because the neutrino self-coupling is still large compared to ω for high energy neutrinos, specifically $\mu\left(r\right) > \omega_{\rm pr}$ after the resonance region. This allows the high energy neutrinos to briefly form a Regular Precession mode before $\mu\left(r\right)$ decreases further with radius and flavor transformation in the $\delta m^2_{\rm atm}$ mixing sector stops.

For the lowest neutrino luminosity, $L_\nu = 1.0 \times 10^{52}\,{\rm erg\,s^{-1}}$, there is no spectral swap observed in Figure 1 between mass states 3 and 2. In this case, $\mu\left(r\right) < \omega_{\rm pr}$ even before the

system finishes MSW-like flavor transformation. No collective oscillation can proceed in the $\delta m^2_{\rm atm}$ mixing sector for this case.

While we have focused entirely on the $\delta m^2_{\rm atm}$ mixing sector in the sections above, it should be pointed out that the $\delta m^2_{\odot}$ mixing sector is completely indifferent to the range of luminosities that we have explored. The neutrino flavor mixing energy scale for the $\delta m^2_{\odot}$ mass state splitting is ~ 30 times smaller than that of the atmospheric mass state splitting. The model of neutrino flavor transformation outlined above is quite robust for the solar mixing sector, with $\mu\left(r\right) > \langle\omega\rangle_{\odot}$ and $\mu\left(r\right) > \left(\omega_{\rm pr}\right)_{\odot}$ for all of the neutrino luminosities that we consider. The spectral swap between mass states 2 and 1 is created by the Regular Precession mode in this mixing sector. While $E_{{\rm swap}_{\odot}}$ varies greatly for the different calculations in Figure 1, this swap energy is only changed by variations in flavor transformation in the $\delta m^2_{\rm atm}$ sector. The ratio of ν_2/ν_1 neutrinos is identical for all of the calculations shown in Figure 1. A curious consequence of this is that the spectral swap energies move closer and closer together as the luminosity of the neutronization burst decreases, until ultimately the swap between mass state 3 and 2 disappears altogether. This behavior is evident in Figure 1.

IV. EXPECTED SIGNAL

So far we have examined the behavior of neutrino flavor transformation in the O-Ne-Mg neutronization burst environment in discreet segments in time, where the neutrino luminosities and spectral energy distributions are fixed. The reality of the neutronization burst is one in which the neutrino emission from the protoneutron star is evolving constantly on time scales which are short compared to the overall length of the burst. The results shown in Figures 1 and 2 are *instantaneous* snapshots of the end results of neutrino flavor transformation during the neutonization burst, and therefore do not necessarily represent the entirety of the expected signal. The luminosities, average energies, and relative fluxes of different flavors of neutrinos emitted during the burst change over the course of the neutronization epoch. Based on our analysis, we conclude that it is possible that these changes could induce significant variation in the flavor swap structure of the neutrino emission over the length of the burst.

Further complicating the issue of what we might expect to see of the neutrino flavor states as they arrive at Earth is that any detected neutronization burst signal will be constructed by

stacking together all of the neutrino events in a detector within some finite window of time. The final result is a time integrated signal where the measured flavor states of individual neutrino energy bins are weighted by their instantaneous fluxes. If the swap structure of the final neutrino flavor states varies widely during this time integration window, the clean flavor swaps show in Figures 1 and 2 may not be easily detectable in the final signal.

To investigate whether these considerations are important, we conducted a suite of multi-angle, 3-flavor, neutrino flavor transformation calculations using the neutronization burst neutrino emission from two separate studies of O-Ne-Mg core-collapse explosions [30, 31]. Starting from the initial rapid rise in $\nu_{\rm e}$ luminosity as the bounce shock moves through the neutrinosphere surface, we solve for the neutrino flavor evolution at six discrete times spaced 5 ms apart after the start of the burst, giving an overall integration time of 30 ms. This section of time slices covers what is broadly defined as the neutronization burst. Although the total length of the neutronization burst is not identical between the two studies, we choose the point of view of an observer who must make a single, appropriate time cut in order to analyze the received signal. To construct our initial neutrino emission spectra for each 5 ms time slice, we take a time average of the luminosity and average neutrino energy for each $\nu/\bar{\nu}$ flavor in a given time slice and use those data to reconstruct overall energy spectra. The neutrino mixing parameters employed for this calculation are the same as those stated at the beginning of this paper when performing calculations for the normal neutrino mass hierarchy. We also treat flavor transformation for neutrinos in the inverted neutrino mass hierarchy, where $\Delta m^2_{\rm atm} = -2.4 \times 10^{-3}\,{\rm eV}^2$.

The normalized total flux of neutrinos found in the final signal is taken to be the time integrated sum of the neutrino flavor states and fluxes produced by each of our calculations. Results for these calculations presented in the vacuum mass basis can be seen in Figures 6 and 7 for the normal neutrino mass hierarchy, and Figures 8 and 9 for the inverted neutrino mass hierarchy. The neutrino flavor basis representation for these results is given in Figures 10 and 11 for the normal neutrino mass hierarchy, and Figures 12 and 13 for the inverted neutrino mass hierarchy.

For neutrinos in the normal mass hierarchy, one can clearly see in Figure 6 that for a neutronization burst of the type found in [30], the swap structures are noticeably disrupted by the time integration of the received neutrino signal. The remnants of the two expected flavor swaps can be seen at ~ 15 MeV and ~ 20 MeV, but these have been smoothed out by

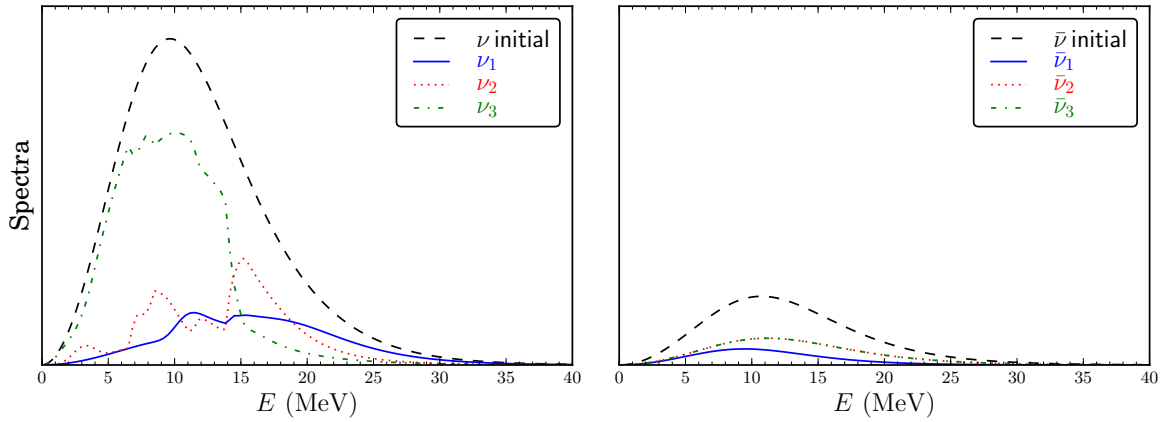

FIG. 6: The expected signal from the neutronization burst of Ref. [30], in the normal neutrino mass hierarchy, created by integrating the final emission angle averaged neutrino spectral energy distribution and fluxes over the first 30 ms of the neutrino burst signal. Left: Scaled neutrino number flux, summed over all neutrino flavors, shown in the vacuum mass basis. Right: Scaled anti-neutrino number flux, summed over all neutrino flavors, shown in the vacuum mass basis.

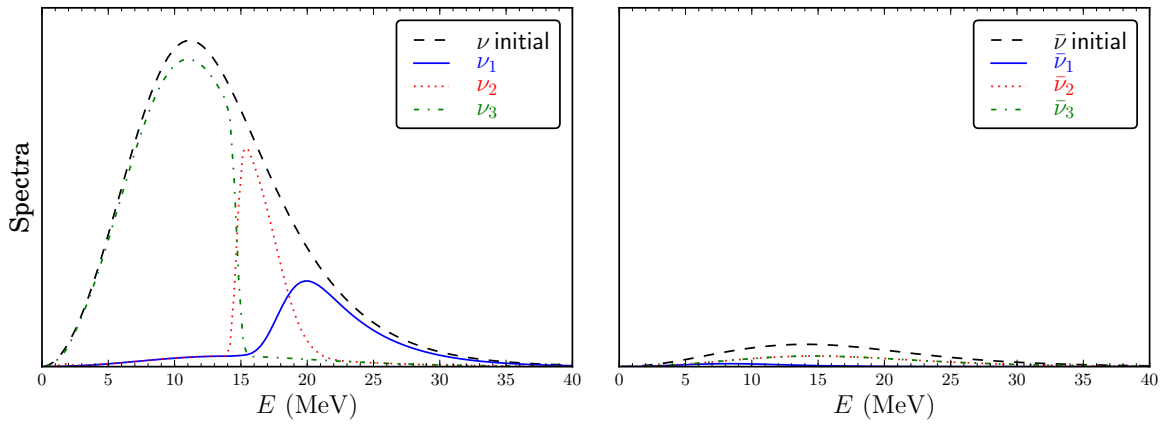

FIG. 7: The expected signal from the neutronization burst of Ref. [31], in the normal neutrino mass hierarchy, created by integrating the final emission angle averaged neutrino spectral energy distribution and fluxes over the first 30 ms of the neutrino burst signal. Left: Scaled neutrino number flux, summed over all neutrino flavors, shown in the vacuum mass basis. Right: Scaled anti-neutrino number flux, summed over all neutrino flavors, shown in the vacuum mass basis.

variations over time. By contrast, Figure 7 shows that for a neutronization burst of the type found in [31], the flavor swap signal remains sufficiently constant throughout the duration

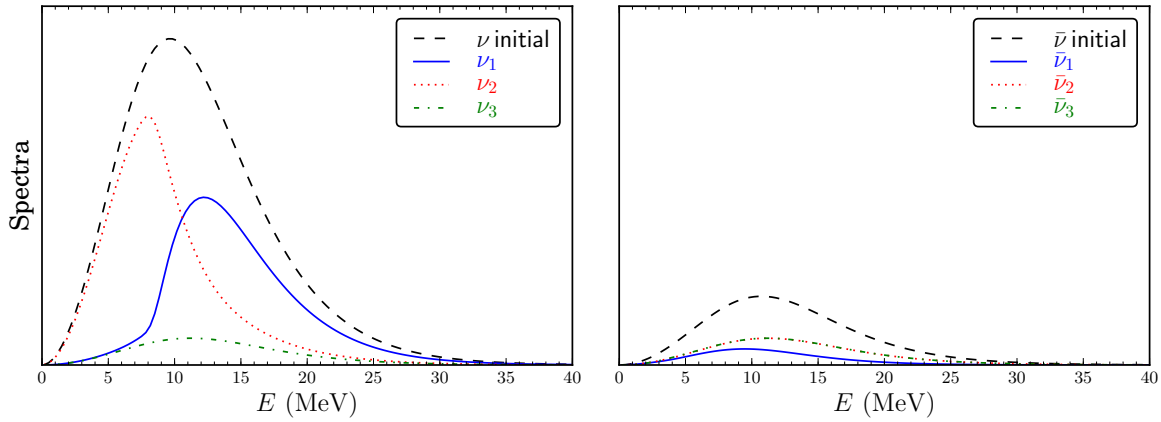

FIG. 8: The expected signal from the neutronization burst of Ref. [30], in the inverted neutrino mass hierarchy, created by integrating the final emission angle averaged neutrino spectral energy distribution and fluxes over the first 30 ms of the neutrino burst signal. Left: Scaled neutrino number flux, summed over all neutrino flavors, shown in the vacuum mass basis. Right: Scaled anti-neutrino number flux, summed over all neutrino flavors, shown in the vacuum mass basis.

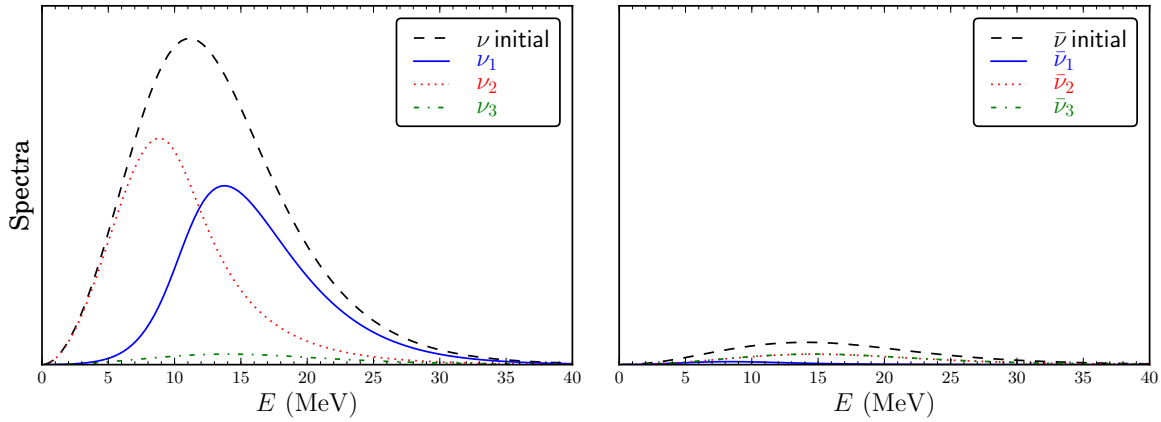

FIG. 9: The expected signal from the neutronization burst of Ref. [31], in the inverted neutrino mass hierarchy, created by integrating the final emission angle averaged neutrino spectral energy distribution and fluxes over the first 30 ms of the neutrino burst signal. Left: Scaled neutrino number flux, summed over all neutrino flavors, shown in the vacuum mass basis. Right: Scaled anti-neutrino number flux, summed over all neutrino flavors, shown in the vacuum mass basis.

of the burst, with a mass state ν_3/ν_2 swap at 14.5 MeV and a mass state ν_2/ν_1 swap at 19 MeV.

The difference in the results for these two models derives from differences in the luminosities and average energies of neutrino emission during the neutronization neutrino burst, which in turn arrises from uncertainties in current models of supernova explosion physics. The neutrino emission parameters given in Ref. [30] are for the lab frame while those in Ref. [31] are for a frame comoving with an infalling mass element. However, even after correcting for the difference between the reference frames, significant differences remain in the neutrino emission parameters for the two supernova models, especially in terms of the neutrino luminosity. We consider that such differences are most likely due to the different physics input used by these two models. In any case, we wish to explore how small but significant variations of neutrino emission affect the signal through collective oscillations. So we have adopted the neutrino emission parameters given in Refs. [30] and [31] as examples. The study in Ref. [30] employs a model which produces $\nu_{\rm e}$'s which have relatively lower average energies, making them more susceptible to luminosity and bump modification of the swap signal over time compared to $\nu_{\rm e}$'s produced in Ref. [31]. Furthermore, the overall fluence of electron lepton number during the neutronization burst epoch in Ref. [30] is less than Ref. [31], which provides a lower relative $\nu_{\rm e}$ luminosity. This in turn makes the swap signal produced in the neutronization burst more variable with time for the neutronization burst in Ref. [30].

For neutrinos in the inverted mass heirarchy, Figures 8 and 9 show that the swap signal is consistent over time for both models we consider. For both studies, the expected neutrino signal has a clear mass state ν_2/ν_1 swap. The swap energies are slightly different, owing to the different average energies of $\nu_{\rm e}$'s in both studies. The swap signals in the inverted neutrino mass hierarchy are insensitive to the differences in neutrino emission between these studies because the inverted mass hierarchy forms only a single swap at the $\Delta m^2_{\odot}$ scale. Because the mass squared splitting for this scale is ~ 30 times smaller than the atmospheric scale, the $\nu_{\rm e}$ luminosity for both of these studies is firmly in the "high luminosity" limit for swap formation via the mode of collective neutrino flavor transformation we have outlined here and, as a result, is not sensitive to the changes in neutrino luminosity and average energy over the course of the burst.

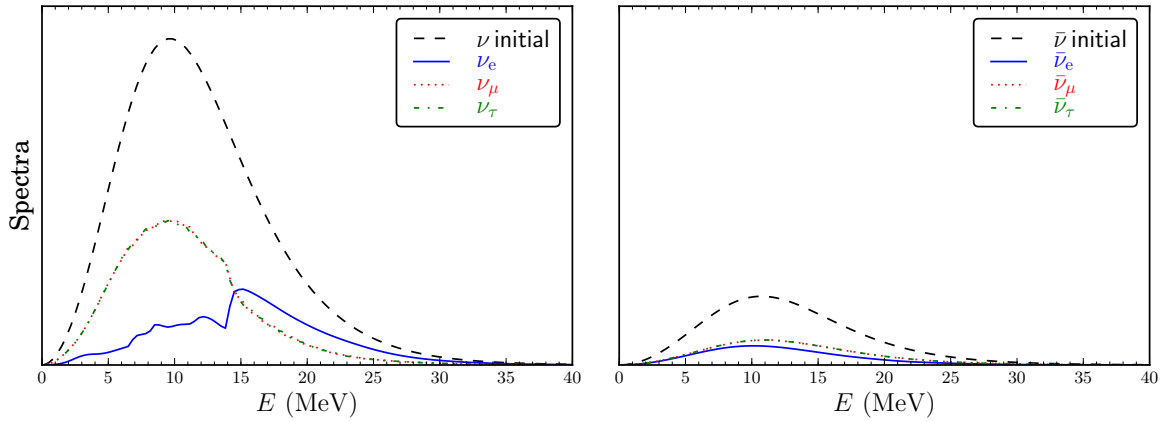

FIG. 10: The expected signal from the neutronization burst of Ref. [30], in the normal neutrino mass hierarchy, created by integrating the final emission angle averaged neutrino spectral energy distribution and fluxes over the first 30 ms of the neutrino burst signal. Left: Scaled neutrino number flux, summed over all neutrino flavors, shown in the neutrino flavor basis. Right: Scaled anti-neutrino number flux, summed over all neutrino flavors, shown in the neutrino flavor basis.

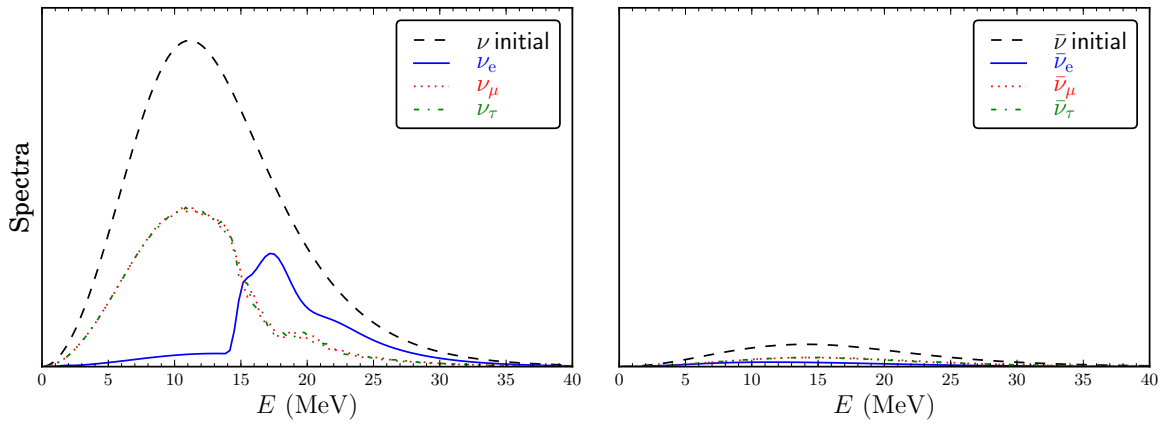

FIG. 11: The expected signal from the neutronization burst of Ref. [31], in the normal neutrino mass hierarchy, created by integrating the final emission angle averaged neutrino spectral energy distribution and fluxes over the first 30 ms of the neutrino burst signal. Left: Scaled neutrino number flux, summed over all neutrino flavors, shown in the neutrino flavor basis. Right: Scaled anti-neutrino number flux, summed over all neutrino flavors, shown in the neutrino flavor basis.

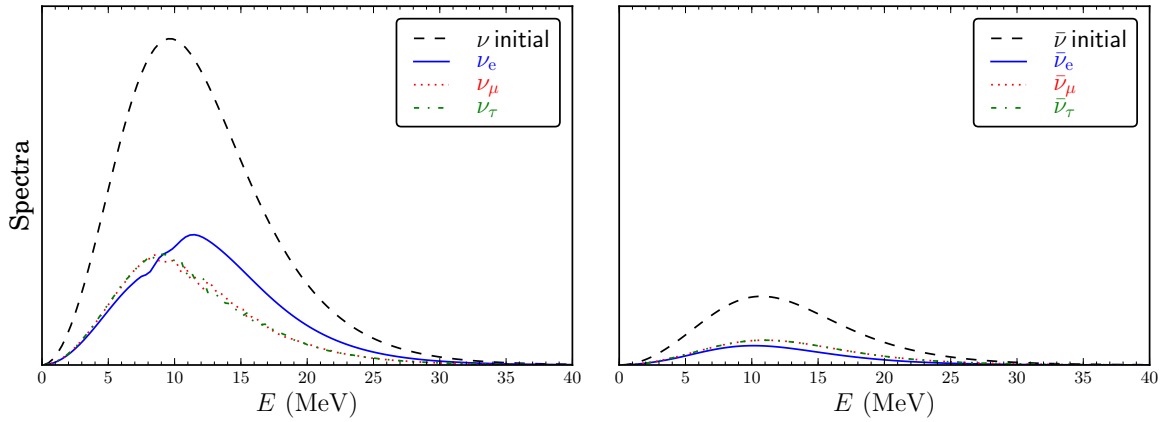

FIG. 12: The expected signal from the neutronization burst of Ref. [30], in the inverted neutrino mass hierarchy, created by integrating the final emission angle averaged neutrino spectral energy distribution and fluxes over the first 30 ms of the neutrino burst signal. Left: Scaled neutrino number flux, summed over all neutrino flavors, shown in the neutrino flavor basis. Right: Scaled anti-neutrino number flux, summed over all neutrino flavors, shown in the neutrino flavor basis.

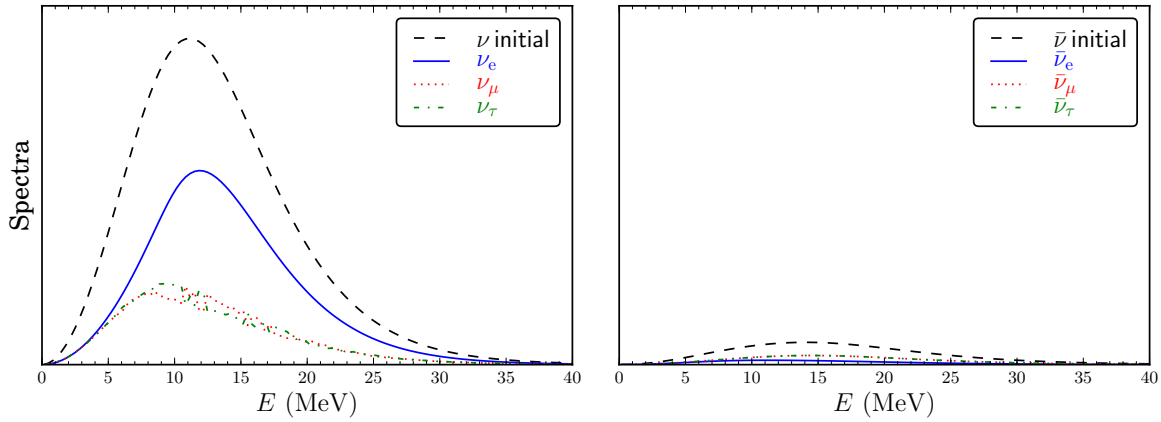

FIG. 13: The expected signal from the neutronization burst of Ref. [31], in the inverted neutrino mass hierarchy, created by integrating the final emission angle averaged neutrino spectral energy distribution and fluxes over the first 30 ms of the neutrino burst signal. Left: Scaled neutrino number flux, summed over all neutrino flavors, shown in the neutrino flavor basis. Right: Scaled anti-neutrino number flux, summed over all neutrino flavors, shown in the neutrino flavor basis.

V. DISCUSSION AND CONCLUSIONS

We have shown that the bump in the electron number density profile at the base of the hydrogen envelope in O-Ne-Mg core-collapse supernovae has important effects in the flavor evolution of low-energy ν_e during the neutronization burst epoch. The bump allows a significant fraction of the low-energy ν_e to remain in the electron flavor state, i.e., enhancing their survival probability. It does this by rendering their flavor evolution nonadiabatic. Additionally, we have found that increasing the luminosity L_ν of the neutronization burst shifts the bump-affected ν_e to lower energy with consequently reduced survival probability. Finally, we have found that the flavor states of the bump affected low energy neutrinos impact the spectral swap forming behavior of the collective oscillations later on. This opens up the possiblity that the presence of bump affected low-energy ν_e of $\sim$ 3–5 MeV can be detected through the spacing of the spectral swaps. However, this may not be necessary as some neutronization burst signals may produce bump affected neutrinos at energies that are accessible by Earth based detectors. This may also prove to be an interesting secondary probe of the burst luminosity L_ν of an O-Ne-Mg core-collapse supernova.

While the zeroth-order mean field proves to be rather useful in understanding the flavor evolution of the low-energy ν_e, it is clearly inadequate in providing a quantitative description of the flavor evolution if the ν_e burst luminosities are on the low side of the expected emission (see Figure 5). In particular, it cannot provide a good estimate for the energy at which the spectral swap occurs in the low luminosity limit. We note that the spectral swap occurs rather robustly at a fixed energy once L_ν exceeds $\sim \sqrt{10} \times 10^{52}$ erg/s (see Figure 1).

We have used these insights to construct the first time integrated neutrino flavor transformation signals of the neutronization burst epoch. These have shown that matter and luminosity induced flavor transformation effects can have significant impact on the neutrino signal that would be received by a detector here on Earth. Neutrinos in the inverted mass hierarchy produce a robust and unique swap signal that is distinct from any signal produced by neutrinos in the normal mass hierarchy, especially in light of mounting evidence that θ_{13} is close to the value used in this paper [32]. Nonetheless, different supernova models give slightly different emission parameters for the neutronization burst. Such differences might be caused by differences in the various physics input used. Most interestingly, these small differences in neutrino emission can cause drastically different spectral changes in the signals

through collective oscillations. Therefore, in addition to probing the fundamental properties of neutrinos, future detection of the neutronization burst from an O-Ne-Mg core-collapse supernova may also provide a venue to test the physics of the supernova explosion outside the neutrino sector.

VI. ACKNOWLEDGMENTS

We thank Tobias Fischer for providing the neutrino emission parameters from his model. This work was supported in part by NSF grant PHY-06-53626 at UCSD, DOE grant DE-FG02-87ER40328 at the UMN, and by the DOE Office of Nuclear Physics, the LDRD Program and Open Supercomputing at LANL, and an Institute of Geophysics and Planetary Physics/LANL minigrant. We would like to thank the topical collaboration for neutrino and nucleosynthesis in hot and dense matter at LANL and the New Mexico Consortium for providing a stimulating platform to carry out this work.

---

[1] K. Nomoto, Astrophys. J. **277**, 791 (1984).

[2] K. Nomoto, Astrophys. J. **322**, 206 (1987).

[3] R. Mayle and J. R. Wilson, Astrophys. J. **334**, 909 (1988).

[4] F. S. Kitaura, H. Janka, and W. Hillebrandt, Astron. Astrophys. **450**, 345 (2006), arXiv:astro-ph/0512065.

[5] H. Duan, G. M. Fuller, J. Carlson, and Y.-Z. Qian, Physical Review Letters **100**, 021101 (2008), 0710.1271.

[6] B. Dasgupta, A. Dighe, A. Mirizzi, and G. G. Raffelt, Phys. Rev. D **77**, 113007 (2008), 0801.1660.

[7] J. F. Cherry, G. M. Fuller, J. Carlson, H. Duan, and Y.-Z. Qian, Phys. Rev. D **82**, 085025 (2010), 1006.2175.

[8] J. F. Cherry, M.-R. Wu, J. Carlson, H. Duan, G. M. Fuller, and Y.-Z. Qian, Phys. Rev. D **84**, 105034 (2011), 1108.4064.

[9] G. M. Fuller, R. W. Mayle, J. R. Wilson, and D. N. Schramm, Astrophys. J. **322**, 795 (1987).

[10] D. Nötzold and G. Raffelt, Nuclear Physics B **307**, 924 (1988).

[11] J. Pantaleone, Phys. Rev. D **46**, 510 (1992).

[12] G. M. Fuller, R. Mayle, B. S. Meyer, and J. R. Wilson, Astrophys. J. **389**, 517 (1992).

[13] Y.-Z. Qian, G. M. Fuller, G. J. Mathews, R. W. Mayle, J. R. Wilson, and S. E. Woosley, Physical Review Letters **71**, 1965 (1993).

[14] S. Samuel, Phys. Rev. D **48**, 1462 (1993).

[15] Y.-Z. Qian and G. M. Fuller, Phys. Rev. D **51**, 1479 (1995), arXiv:astro-ph/9406073.

[16] V. A. Kostelecký and S. Samuel, Phys. Rev. D **52**, 621 (1995), arXiv:hep-ph/9506262.

[17] S. Samuel, Phys. Rev. D **53**, 5382 (1996), arXiv:hep-ph/9604341.

[18] S. Pastor and G. Raffelt, Physical Review Letters **89**, 191101 (2002), arXiv:astro-ph/0207281.

[19] S. Pastor, G. Raffelt, and D. V. Semikoz, Phys. Rev. D **65**, 053011 (2002), arXiv:hep-ph/0109035.

[20] R. F. Sawyer, Phys. Rev. D **72**, 045003 (2005), arXiv:hep-ph/0503013.

[21] G. Fogli, E. Lisi, A. Marrone, and A. Mirizzi, Journal of Cosmology and Astro-Particle Physics **12**, 10 (2007), 0707.1998.

[22] A. B. Balantekin and Y. Pehlivan, Journal of Physics G Nuclear Physics **34**, 47 (2007), arXiv:astro-ph/0607527.

[23] J. Gava, J. Kneller, C. Volpe, and G. C. McLaughlin, Physical Review Letters **103**, 071101 (2009), 0902.0317.

[24] H. Duan, G. M. Fuller, and Y.-Z. Qian, Annual Review of Nuclear and Particle Science **60**, 569 (2010), 1001.2799.

[25] J. Kneller and C. Volpe, Phys. Rev. D **82**, 123004 (2010), 1006.0913.

[26] A. B. Balantekin, ArXiv e-prints (2011), 1111.2282.

[27] Y. Pehlivan, A. B. Balantekin, T. Kajino, and T. Yoshida, Phys. Rev. D **84**, 065008 (2011), 1105.1182.

[28] K. Nakamura and Particle Data Group, Journal of Physics G Nuclear Physics **37**, 075021 (2010).

[29] H. Duan, G. M. Fuller, and Y.-Z. Qian, Phys. Rev. D **74**, 123004 (2006), arXiv:astro-ph/0511275.

[30] C. Lunardini, B. Müller, and H. Janka, Phys. Rev. D **78**, 023016 (2008), 0712.3000.

[31] T. Fischer, S. C. Whitehouse, A. Mezzacappa, F.-K. Thielemann, and M. Liebendörfer, Astronomy and Astrophysics **517**, A80 (2010), 0908.1871.

[32] F. P. An, J. Z. Bai, A. B. Balantekin, H. R. Band, D. Beavis, W. Beriguete, M. Bishai, S. Blyth, R. L. Brown, G. F. Cao, et al., ArXiv e-prints (2012), 1203.1669.